**Lionel E. Edwin**
Mechanical and Aerospace Engineering,
North Carolina State University,
Raleigh, NC 27695
e-mail: ledwin@ncsu.edu

**Jason D. Denhart**
Mechanical and Aerospace Engineering,
North Carolina State University,
Raleigh, NC 27695
e-mail: jddenhar@ncsu.edu

**Thomas R. Gemmer**
Mechanical and Aerospace Engineering,
North Carolina State University,
Raleigh, NC 27695
e-mail: trgemmer@ncsu.edu

**Scott M. Ferguson**
Assistant Professor
Mechanical and Aerospace Engineering,
North Carolina State University,
Raleigh, NC 27695
e-mail: scott_ferguson@ncsu.edu

**Andre P. Mazzoleni**
Associate Professor
Mechanical and Aerospace Engineering,
North Carolina State University,
Raleigh, NC 27695
e-mail: a_mazzoleni@ncsu.edu

# Performance Analysis and Technical Feasibility Assessment of a Transforming Roving-Rolling Explorer Rover for Mars Exploration

*This paper explores a two state rover concept called the Transforming Roving-Rolling Explorer (TRREx). The first state allows the rover to travel like a conventional 6-wheeled rover. The second state is a sphere to permit faster descent of steep inclines. Performance of this concept is compared to a traditional rocker-bogie (RB) architecture using hi-fidelity simulations in Webots. Results show that for missions involving very rugged terrain, or a considerable amount of downhill travel, the TRREx outperforms the rocker-bogie. Locomotion of the TRREx system using a continuous shifting of the center of mass through "actuated rolling" is also explored. A dynamics model for a cylindrical representation of the rover is simulated to identify feasible configurations capable of generating and maintaining continuous rolling motion even on sandy terrain. Results show that in sufficiently benign terrain gradual inclines can be traversed with actuated rolling. This model allows for increased exploration of the problem's design space and assists in establishing parameters for an Earth prototype.* [DOI: 10.1115/1.4027336]

## 1 Introduction

The challenges of designing robotic rovers for planetary surface exploration are considerable. While the first Lunar rovers could be controlled in near real-time [1], Martian rovers must be at least semi-autonomous [2]. Further, since the Martian terrain is severely chaotic [3] rovers must operate in environments characterized by unknown rock fields, various soil types, crevices, and significant changes in slope.

All successful rover missions to Mars have used six wheeled RB suspension systems. First used as the suspension for the Sojourner microrover in 1997 [4], rocker-bogie suspensions consist of a differential mechanism (the "rocker") joining one wheel to a bogie that holds two more wheels. This suspension system allows all six wheels to remain in contact with the ground, reduces the likelihood of wheel sinkage, and increases the ability for all wheels to contribute to propulsion [5]. This architecture also allows the wheels to undergo a large amount of articulation with a rigid suspension, allowing scientific instruments to remain relatively stable when roving.

Rovers previously sent to Mars had missions deliberately chosen to avoid impassable terrain [6]. Multistage bogie systems have been proposed to provide greater weight distribution capabilities and articulation by connecting bogies in series [2,7]. However, rocker-bogie designs have difficulty navigating steep crater walls and are limited to speeds below 10 cm/s due to dynamic interactions that severely impact rover stability [8]. Traversing significant slopes (>10 deg) can also pose difficulties, with slippage of up to 91% of the total distance traveled on slopes of 20 deg reported. These rovers also experienced as much as 10–20 deg of yaw when traversing large obstacles [9].

In an effort to explore novel rover architectures, the TRREx rover has been developed at NC State [10]. The hypothesis behind this new configuration is that by rolling down hills, the limitations of a traditional rocker-bogie can be relaxed. This concept can reconfigure [11] into two distinct states: a roving mode employing a form of active suspension to move on six wheels, and a rolling mode that allows it to roll down slopes in the form of a sphere. An illustrative example of this configuration change is shown in Fig. 1.

This paper explores the technical feasibility of the TRREx concept and assesses performance in comparison to a traditional rocker-bogie architecture. A hi-fidelity simulation environment is used to run a battery of test scenarios representing different ground tractions, slopes, and rock field densities. Actuated rolling in the rolling state is studied using a cylindrical model of the system to generate insights into the relationships between the design and the friction, slopes, and obstacles that it could overcome. Finally, this paper explores how the design parameters might be tuned to improve mobility and aid the sizing of actuators and sensors for a physical prototype.

## 2 Background

This section provides background on reconfigurability in engineering design research and discusses using simulation environments to measure spacecraft system performance.

**2.1 Reconfigurability in Complex Engineered Systems.** In the last 10 years the engineering design community has begun

Contributed by the Design Automation Committee of ASME for publication in the Journal of Mechanical Design. Manuscript received June 7, 2013; final manuscript received March 27, 2014; published online May 5, 2014. Assoc. Editor: Irem Y. Tumer.

  

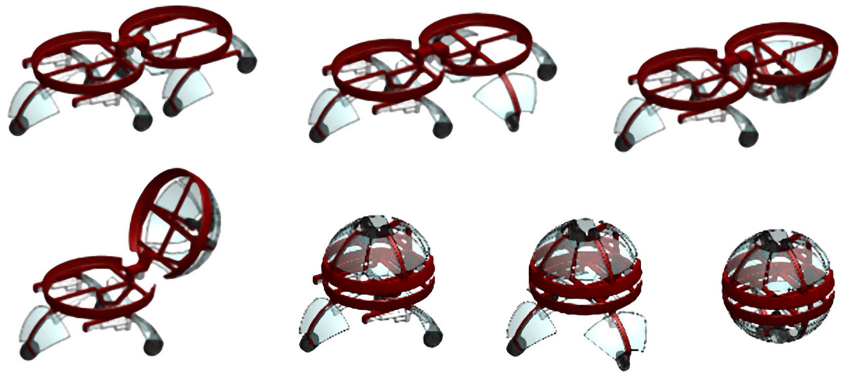

**Fig. 1 TRREx rover configuration change**

exploring the benefits of changeable and reconfigurable systems [11]. Research supporting the brainstorming and early conceptual phases of design has identified four transformation principles [12–14] that fundamentally describe how systems change in service. Numerical studies have focused on the need to accommodate multiple abilities and are motivated by the inherent tradeoffs that must be navigated [11,15,16]. Interest in this area has also led to a desire for engineered resilience [17,18], or the ability to affordably adapt and effectively perform across wide ranges of operational contexts.

Efforts assessing the performance advantage associated with reconfigurability began with parameter studies [19,20], multiobjective formulations for end-state determination [15,20–24], and the development of probabilistic models to predict when state modifications should occur [25,26]. More advanced techniques have relied on the assignment of cost data [15,22], modular expansion [27–31], product family generation [32–34] and the generalization of a linear tracking control scheme with assumed system dynamics [35]. These numerical-based explorations are in line with the position taken by McGowan et al. [36], who state that it is inefficient to devote a large amount of resources in the early stages of design to modeling the detailed interactions between system architecture and the act of reconfiguration.

The works cited above commonly use repeatable, consistent simulations and analytical equations to represent objective functions and system behavior. Assessing the performance of a rover concept is challenging because mobility in chaotic terrain is characterized by uncertainty and randomness, leading to an infinite number of possible simulation scenarios. This paper extends the analysis of reconfigurable systems by exploring performance when the simulation is nonrepeatable and exploring the dynamics associated with a cylindrical model of the system.

**2.2 Using Simulations to Assess Spacecraft Performance.** Computer simulations can facilitate comparative studies of complex systems without the investment required for scaled prototyping. While analytical models and simulations do have possible limitations—reduced accuracy, can be based on approximations, unexpected interactions may not be modeled—environments like the Rover Analysis Modeling and Simulation (ROAMS) software [37] and the Rover Chassis Evaluation Tool (RCET) have demonstrated their applicability for evaluating and optimizing space exploration rovers [38]. ROAMS and RCET allow specialized, hi-fidelity simulations of rover operations that include everything from electrical system modeling to complex wheel-terrain interaction models [39,40]. A good virtual simulation environment for planetary rovers only *needs* to include a 3D terrain model, a rover dynamic model, and accurate dynamic interactions between the two [41]. COSMOS®, is one example of a general use software package that can provide these capabilities [42].

The commercial robotics package Webots™ is used in this work as the primary simulation engine [43–45], because it offers large scale modeling capabilities using simplified rover architectures. Rover models can be built in a simple computer-aided design environment from solid elements connected by joints with servos, actuators, sensors, etc. that are controlled via customized C-based controllers. Webots can model a variety of terrain by using stationary rigid bodies to simulate terrain elements, varying the coulomb friction coefficient between the rover and the terrain, and changing the gravity vector. These features allow the rovers to be tested in an environment that approximates their eventual mission conditions. Terrain-rover interactions are carried out using the open dynamics engine [46], allowing more complicated dynamics to be added if future work requires them.

Simulations of highly complicated rovers are often limited to the detailed kinematics and control schemes that are involved in the operation of a single rover type [47–49]. This involves direct solution of the Newton-Euler or Lagrangian dynamics equations for the rover. Detailed modeling of this type is also valuable, and indeed necessary, in evaluating potential rover designs [50]. This has already been addressed in the literature in detail for many variations and adaptations of rocker-bogie suspension rovers [51,52]. The kinematics model for the TRREx system is introduced and described in Sec. 4. In this paper, simulations are used to conduct a comparative study between the rocker-bogie architecture and the TRREx across a variety of terrain types. Performance of each architecture is then assessed and compared. The methodology behind these simulations is discussed in Sec. 3.

## 3 Initial Feasibility Study of the TRREx Concept

The TRREX concept is an early conceptual design in that there is a general understanding of system layout and a high-level description of how the system might reconfigure. However, moving toward an embodied concept requires choosing and defining components, establishing detailed system dimensions, and exploring the desired reconfigurations. Before dedicating the resources needed to embody the concept, initial performance and technical feasibility assessments should be completed to ensure that the concept is viable. The objective of this section is to present the experimental setup used to compare the TRREx concept with a traditional rocker-bogie design. Results obtained from this process will then be described to assess the performance advantages of the TRREx rover.

**3.1 Experimental Setup.** Four rovers—each concept at full scale and half scale—are tested by creating models of each in Webots, as shown in Fig. 2. At full scale the rocker-bogie rover was modeled to be the same size as the Curiosity rover: approximately 3 m from the front wheel to the back and 3 m wide. The TRREx concept was scaled to be approximately the same size as

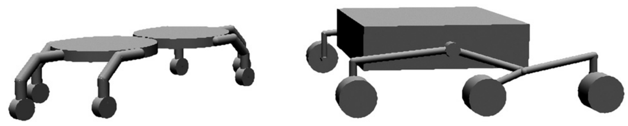

**Fig. 2 Testing models used in Webots, TRREx (left), and rocker-bogie (right)**

**Table 1 Terrain parameters**

| Level | Slope | Rock field distribution | Friction |
|---|---|---|---|
| 1 | 30 deg uphill | Sparse | High |
| 2 | 15 deg uphill | Dense | Low |
| 3 | 0 deg | — | — |
| 4 | 15 deg downhill | — | — |
| 5 | 30 deg downhill | — | — |

the rocker-bogie model. The roving mode of the TRREx is approximately 3 m from front wheel to rear wheel, and 1 m across at the wheels. At this scaling, the TRREx in rolling mode is a 1 m sphere. The rolling mode of the TRREx concept was modeled as a solid sphere on the assumption that all necessary hardware are internally packaged in rolling mode with a center of gravity position in the center of the sphere. This assumption may be relaxed in future works.

A battery of trial environments 8 m wide and 25 m long were created to test rover performance along a straight line course. The rovers were started 2.5 m along the length, in the center of the width, and were pointed at a target 20 m directly ahead. This allowed assessment of each concept's essential characteristics without requiring complicated control schemes to be modeled, and provides insight into how much control would be needed in different scenarios. As the system models are developed further in future work, control complexity can be added as an additional performance measure or tradeoff parameter.

*3.1.1 Terrain Characteristics.* Angle of ascent/descent, traction, and rock field density were selected as the terrain variables for this study, as shown in Table 1. Angle of ascent/descent refers to the angle the ground makes with a plane perpendicular to the gravity vector. The rover starts pointed straight up (or down) the slope of this hill. While local anomalies may create small features with steeper than 30 deg slopes, studies have suggested that it is unlikely that large features with uniformly steeper slopes exist on Mars [53]. Since a fully capable robot could navigate around a localized trouble spot, this investigation was bounded to slopes less than or equal to 30 deg.

The distribution and size of the rock field was governed by Eq. (1), where $N$ is the cumulative number of rocks per square meter with a diameter greater than or equal to a given diameter, $D$ (in meters) [54].

$$N(D) = Le^{-sD} \tag{1}$$

The diameter distribution is based on input parameters $L$ and $s$, the dimensions of the desired field and the slope angle. A "sparse" field was generated using information from the Viking 2 lander site ($L = 6.84$, $s = 8.3$). The "dense" field was generated using information for Mars Hill, a testing site in Death Valley, CA which is quite rugged in comparison ($L = 4.78$, $s = 3.06$). Sparse and dense are relative terms used for the purpose of this study, as the Viking 2 lander site is believed to be amongst the rockiest places on Mars. Mars Hill, meanwhile, is likely to be more rugged than any location on Mars. It is included in this trial to push the limits of the rover architectures. Terrain was generated using randomly assigned rock diameters and locations, and rocks were modeled as spheres with their centers lying in the plane of the sloped ground.

Finally, while a soil model capable of representing sinking and slipping is a source of future work, the studied ground interaction only includes a slipping model. Soil strength is often modeled starting with Eq. (2) [55]

$$\tau_{\max} = c + \sigma \tan \phi \tag{2}$$

In this equation, $\tau_{\max}$ is the maximum shear stress the soil can sustain, $c$ is the cohesitivity, $\sigma$ is the normal stress on the soil, and $\phi$ is the soil's friction angle. Since sinking was not considered, and Martian soil has very low cohesitivity [53], $c$ was removed from the analysis. Rearranging the terms yields

$$C_f = \frac{\tau}{\sigma} = \tan\,\phi \tag{3}$$

In above equation, $C_f$ is the friction coefficient. Two values of $\phi$ were chosen for the ground-wheel interaction. "Low" friction is modeled as $C_f = \tan$ (17 deg). This is in the range given for dust deposits. "High" friction is modeled as $C_f = \tan$ (38 deg) which is consistent with dust overlying rock [53].

*3.1.2 Experimental Process.* Twenty test scenarios were created by enumerating the full factorial of possible combinations of the three terrain variables shown in Table 1. All rovers were operated at a constant 2.5 cm/s on flat ground. This is representative of a mid-range speed for Mars rovers, although they are usually operated closer to 1 cm/s since large parts of their control is done on Earth. Rover location was reported every 10 s during the simulation.

In several cases, a rover would completely fail a trial. One failure scenario involved a disruption of rover orientation that was significant enough to cause the system to exit the field before reaching the end target. Triggering this failure mode represented the need for a command input capable of returning the rover to its desired path. Other sources of failure included a rover partially surmounting an obstacle but getting stuck, encountering an obstacle it simply could not overcome, and not making forward progress uphill, or not preventing an uncontrolled downhill slide, because of insufficient friction with the ground. When any of these failures occurred, a note was made in the data set and the rover was manually moved past the obstacle, allowing the rover to be evaluated across multiple field sections.

*3.1.3 Measuring System Performance.* The most basic description of performance might be "How far did the rover go?" Mathematically, this is the straight line distance from the start point to the point where the rover stops. However, this metric is not robust in the context of a randomly distributed rock field. For instance, a large rock in close proximity to the starting location can end a trial before much data are collected. To overcome this limitation, a rover encountering a failure was reset and moved over the obstacle causing the failure. The trial resumed from there, and the data were broken into forward progress segments by identifying where the rover started and stopped. In this way, multiple trials were performed.

Three performance measures using the raw position data were obtained from the Webots simulations. The first measure was based on mean free path (MFP), which is defined as "expected distance that the vehicle can travel in a straight line before it encounters a nontraversable hazard," and has been used to classify the rover's intrinsic ability to overcome obstacles [42]. While MFP can be analytically calculated using the rock distribution with a rock size that the rover cannot overcome, it was measured directly in this study as the average of the stopping points in the Webots simulations. However, MFP can be susceptible to noise when the number of simulations is small.

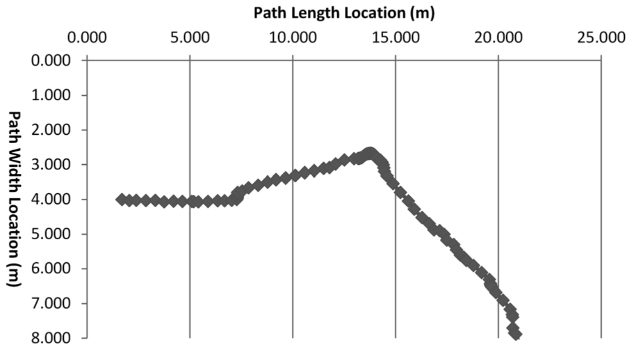


**Fig. 3 Raw data from Webots simulations**

The sophistication of the control scheme need for the rover can be approximated when the MFP is divided by the rover's minimum turning circle. This is the mean free path ratio (MFPR), and when MFPR is larger than one a rover should need only occasional course corrections and high-level navigation inputs. If the MFPR is much smaller than one, the rover is incapable of navigating in the terrain under consideration. For a rover with MFPR near one, mobility is possible but requires detailed sensing and sophisticated navigational control [42].

A second performance measure is the root mean square distance from the path ($D_{rms}$). It is calculated for each data point using Eq. (4), where $z_{rover}$ is the coordinate of the rover as it deviates from its intended centerline travel direction and $z_{path}$ is the location of the straight line from the start to the finish.

$$D_{z,rms} = \sqrt{\mathrm{mean}((z_{rover} - z_{path})^2)} \quad (4)$$

$D_{rms}$* provides a different measure of control input required by characterizing how much the rover moves away from its desired straight path due to the obstacles. To account for possible restarts of a trial, this term is normalized against the MFP. As shown in Eq. (5), $D_{rms}^*$ becomes the ratio of how far the rover moves sideways to how far it moves forward, where the scalar magnification term makes the value larger for computational purposes. Large values of this term are undesirable, and a case where the MFP is equal to zero means that rover did not move from the start point. A system exhibiting this property is essentially uncontrollable and deemed infeasible.

$$D_{rms}* = \frac{10 * D_{z,rms}}{\mathrm{MFP}} \quad (5)$$

Finally, the third performance measure was average speed ($V_{avg}$), as shown in Eq. (6). Since the rovers completed each trial at the same speed, this is a measure of how the rock field hinders the rover's forward progress. For each forward progress segment of the trial, the distance traveled over the $n$ data points is calculated.

$$V_{avg} = \frac{\sum_{i=1}^{n} D_{segment}}{\sum_{i=1}^{n} t_{elapsed}} \quad (6)$$

However, it is likely that the information from these three performance measures may conflict. For such decisions involving multiple criteria, a common procedure is to aggregate strength of preference curves and weights for each attribute [56–59]. For example, research in decision-based-design develops strength of preference (SoP) curves using nondimensional utility curves. The scores of each attribute are then added through the application of a weighting scheme, as shown below

$$V_j = \sum_{i=1}^{3} w_i r_{i,j}(x_{i,j}) \quad (7)$$

In this equation, $V_j$ is the value of the $j$th alternative, $w_i$ is the weight of the $i$th performance measure, $x_{i,j}$ is the level of the $i$th performance characteristic of the $j$th alternative, and $r_{i,j}$ is the nondimensional score as a function of $x_{i,j}$.

For this investigation, it is assumed that the designer's SoP curves are known. The three performance measures, MFPR, $D_{rms}^*$, and $V_{avg}$, are mapped to a nondimensionalized score and the overall value for each trial is aggregated using attribute weights.

**Table 2 Performance ranges**

| Objective | Best observed | Worst observed | $r=1$ | $r=0$ |
|---|---|---|---|---|
| MFPR (unitless) | 20 | 0.05 | 3.5 | 1 |
| $D_{rms}$* (unitless) | 0.045 | 60.5 | 0 | 20 |
| $V_{avg}$, flat/up (m/s) | 0.025 | 0.002 | 0.025 | 0 |
| $V_{avg}$, down (m/s) | 2.66 | 0.01 | 2.7 | 0 |

### 3.2 Architecture Performance Analysis Using Webots.

The objective of this section is to compare the performance of the TRREx architecture and the traditional rocker-bogie architecture. Figure 3 illustrates an example of rover trajectory plotted from the position data obtained from Webots. The horizontal axis is the distance in meters traveled down the intended path, and the vertical axis is the deviation from the centerline.

While various techniques exist for defining SoP curves, linear curves are assumed. To derive the linear relationship between performance measure and nondimensionalized score, a maximum and minimum performance must be defined, as shown in Table 2. For most objectives, these values are set to the best and worst observed value.

A MFPR value of 1 was given the lowest score ($r=0$) because these rovers are capable of maneuvering but require sophisticated control. A rover with a MFPR less than 1 describes a system that is not sufficiently maneuverable to perform the task, thereby making it an infeasible choice. This is consistent with Patel et al.'s categorization of MFPR [42]. Further, a MFPR value of 3.5 was given the highest score ($r=1$) since any value above this should be sufficiently maneuverable without the need for additional control.

A $D_{rms}^*$ performance measure of 20 was used to establish the lower bound for the SoP curve, as a rover with this performance will deviate drastically from its assigned path. Two curves were used for $V_{avg}$ because two distinctly different speed regimes existed. The flat and uphill data were limited by the forward speed of the rover. The downhill speed range had much higher potential due to the freely rolling TRREx in rolling mode. Therefore, a flat/uphill strength of preference curve is used for the flat (trials 9–12) and uphill (trials 1–8) trials, while a downhill strength of preference curve is used or the downhill trials (trials 13–20).

*3.2.1 Initial Weight Scheme Study Using Individual Trials.* A weighting scheme is applied to aggregate the scores from the various SoP curves. Six different weighting schemes, shown in Table 3, are explored in this work. The first four schemes are designed to explore different preference structures for the three performance objectives. The fifth column focuses on ability to stay on the centerline path and complete the course, while the final

Table 3 Weight schemes explored

| Perf. measure | Scheme 1 | Scheme 2 | Scheme 3 | Scheme 4 | Scheme 5 | Scheme 6 |
|---|---|---|---|---|---|---|
| $w_{mfpr}$ | 0.333 | 0.500 | 0.333 | 0.333 | 0.500 | 0.000 |
| $w_{drms}$ | 0.333 | 0.167 | 0.167 | 0.500 | 0.500 | 0.000 |
| $w_{vavg}$ | 0.333 | 0.333 | 0.500 | 0.167 | 0.000 | 1.000 |

Table 4 Number of times identified as best alternative in a trial

| Rover | Scheme 1 | Scheme 2 | Scheme 3 | Scheme 4 | Scheme 5 | Scheme 6 | Total |
|---|---|---|---|---|---|---|---|
| Small TRREx | 5 | 4 | 4 | 5 | 3 | 5 | 26 |
| Large TRREx | 5 | 6 | 6 | 5 | 1 | 7 | 30 |
| Small RB | 3 | 3 | 3 | 3 | 2 | 2 | 16 |
| Large RB | 5 | 5 | 5 | 5 | 12 | 4 | 36 |
| None | 2 | 2 | 2 | 2 | 2 | 2 | 12 |

Table 5. Number of times identified as best alternative per trial slope

| Rover | Uphill | Flat | Downhill |
|---|---|---|---|
| Small TRREx | 13 | 0 | 13 |
| Large TRREx | 0 | 1 | 29 |
| Small RB | 16 | 0 | 0 |
| Large RB | 7 | 23 | 6 |
| None | 12 | 0 | 0 |

column focuses solely on speed. The number of times that each rover was identified as the best alternative for a trial per weight scheme is shown in Table 4. The large rocker bogie architecture has the most number of wins, but this is due to a dominant performance in the fifth weight scheme when performance is solely based on the ability to stay on—and complete—the course. This weight scheme essentially eliminates the advantage of the TRREx reconfiguring from roving to rolling mode by ignoring velocity differences between the architectures.

There were two trials where none of the rover concepts could complete the course. These trials required the rover to go uphill, had dense rocks fields, and low friction values. Across weighting schemes, the results are rather consistent, as one rover configuration usually was the dominant choice for a given trial. When the best alternative did change because of a different weight scheme, it typically involved rover scale rather than architecture. Ignoring the fifth weight scheme, this happened only 5 times (out of 100).

The weighting schemes in Table 3 were chosen to sample different regions of the solution space. Strong statements about the nondominance of an architecture concept for a trial cannot be made because weighted sum techniques do not capture nonconvex regions of the nondominated frontier and do not guarantee an even spacing of solutions. Rather, these results are presented to demonstrate that the TRREx architecture can compete with—or outperform—the rocker-bogie architecture at the level of detail considered in the simulation.

This statement is further supported when the results are separated by the slope of the operating environment. As shown in Table 5, the TRREx rovers are the best alternative for downhill trials because the reconfiguration into rolling mode allows a high performance in the $V_{avg}$ category. The Large RB dominates on flat ground. Small rovers usually are the best alternative for hill climbing because their short turning radii improve their MFPR.

*3.2.2 Performance Assessment Across Various Missions.* The results in Sec. 3.2.1 discussed solutions for individual trials. This section aggregates the trials into a set of missions comprised of various terrain types. For this study, the weights on the performance parameters were set to 1/3. Four hypothetical missions were envisioned and are defined as:

- Mission 1—Mostly flat, sparse terrain with mildly varying slope, friction, and minimal rugged terrain
  - o 50% task 9: flat, high friction, sparse rocks
  - o 10% task 5: 15 deg uphill, high friction, sparse rocks
  - o 10% task 10: flat, low friction, sparse rocks
  - o 10% task 11: flat, high friction, rugged rocks
  - o 10% task 13: 15 deg downhill, high friction, sparse rocks
- Mission 2—Nearly equal amounts uphill and downhill with samplings of terrain of friction settings
  - o 25% task 3: 30 deg uphill, high friction, rugged rocks
  - o 15% task 5: 15 deg uphill, high friction, sparse rocks
  - o 5% task 6: 15 deg uphill, low friction, sparse rocks
  - o 15% task 13: 15 deg downhill, high friction, sparse rocks
  - o 5% task 16: 15 deg downhill, low friction, sparse rocks
  - o 25% task 17: 15 deg downhill, high friction, rugged rocks
  - o 10% task 19: 30 deg downhill, high friction, sparse rocks
- Mission 3—Flat and mild slopes, but with rugged rocks and mostly high friction
  - o 30% task 7: 15 deg uphill, high friction, rugged rocks
  - o 25% task 11: flat, high friction, rugged rocks
  - o 10% task 12: flat, low friction, rugged rocks
  - o 25% task 15: 15 deg downhill, high friction, rugged rocks
  - o 10% task 16: 15 deg downhill, low friction, rugged rocks
- Mission 4—A mix of downhill scenarios
  - o 25% task 13: 15 deg downhill, high friction, sparse rocks
  - o 25% task 15: 15 deg downhill, high friction, rugged rocks
  - o 25% task 17: 30 deg downhill, high friction, sparse rocks
  - o 25% task 19: 30 deg downhill, high friction, rugged rocks

The resulting scores for each mission are shown in Table 6. The first mission is largely comprised of flat terrain where large rocker-bogies demonstrate proficiency. However, the difference between the second and third place alternatives is relatively small. This suggests that there may be tradeoffs worth exploring between the small RB and small TRREx concepts. For the second mission, the small RB concept was the winner. The small TRREx is the only feasible alternative for the trial 7 segment of the third mission, making it the only rover capable of completing this mission. Further, since the TRREx is designed to have an advantage going downhill, it is expected that the TRREx rovers would take the first and second spots in the fourth mission.

Now, suppose that the weights on the performance measure are changed to place a larger emphasis on speed. For example, Mission 2 could be analyzed with a weight scheme of $w = 0.333$ for MFPR, $w = 0.167$ for $D_{rms}^*$, and $w = 0.5$ for $V_{avg}$. As shown in Table 7, the small TRREx would be selected because of the significant score change for the small RB rover. This change in final

**Table 6 Rover performance scores for the four hypothetical missions**

| Rover | Mission 1 | Mission 2 | Mission 3 | Mission 4 |
|---|---|---|---|---|
| Large RB | 0.807 | 0.551 | Insuf | 0.666 |
| Large TRREx | 0.674 | 0.619 | Insuf | 0.830 |
| Small RB | 0.740 | 0.716 | Insuf | 0.571 |
| Small TRREx | 0.730 | 0.672 | 0.511 | 0.776 |

**Table 7 Scores for Mission 2 using a modified weight scheme**

| Rover | Original score | New score | Change in score |
|---|---|---|---|
| Large RB | 0.551 | 0.453 | −0.098 |
| Large TRREx | 0.619 | 0.571 | −0.048 |
| Small RB | 0.716 | 0.589 | −0.127 |
| Small TRREx | 0.672 | 0.603 | −0.069 |

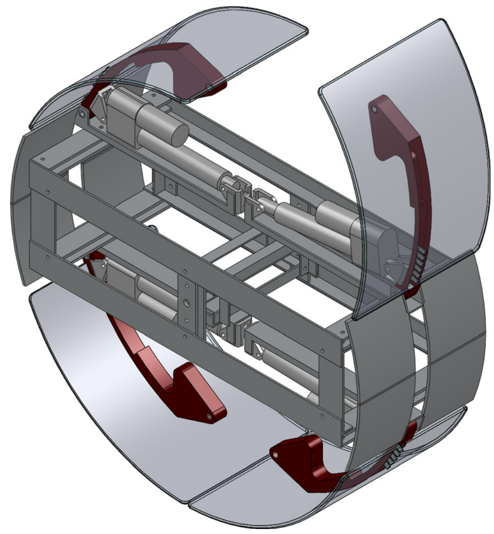

**Fig. 4 Cylindrical version of the TRREx**

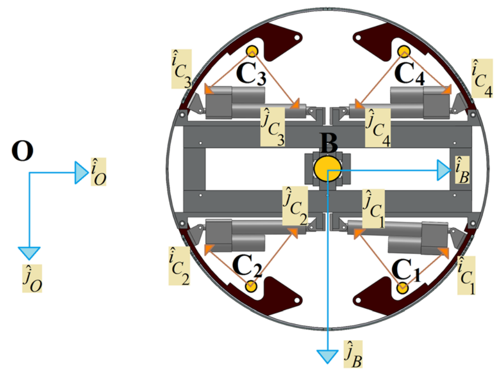


**Fig. 5 Definition of frames**

solution suggests greater variability in the solution space when the trials themselves are aggregated into more complex missions. Since the biggest advantage provided by the TRREx is its increase in downhill speed, it gains significant advantages over the rocker-bogie architecture when missions provide an opportunity for rolling. However, the designer must care sufficiently about speed or the rocker-bogie may be preferred. While studying the variability in the solution space is left for future work, these outcomes support the hypothesis that the TRREx rover is an architecture worthy of additional investigation. Section 4 further advances this concept by exploring the dynamics of the TRREx under actuated rolling.

## 4 Planar Modeling and Analysis of the TRREx Architecture

The results from Sec. 3.2.2 demonstrated that, given an appropriate mission, the TRREx concept may outperform the traditional rocker-bogie architecture. Further, it could be possible that actuated rolling may increase concept value, especially in terrains that do not have a negative gradient. This section explores a cylindrical representation of the system to better understand system dynamics and TRREx capabilities under actuated rolling.

**4.1 Modeling Actuated Rolling of Cylindrical TRREx Model.** Studies of tumbleweed rovers have led to the development of detailed, mathematical models of spherical systems free rolling down an incline [60–63]. These models are capable of representing collisions with rocks and include aerodynamic forces acting on the sphere. Modeling actuated rolling is made more complicated by incorporating control inputs that control the dynamics of the system. To study actuated rolling of the TRREx, a cylindrical (i.e., "planar") version is considered, as shown in Fig. 4, and an appropriate analytical model is developed.

Analyzing a cylindrical representation of the system will help in understanding the inherent relationships between the design of the TRREx rover and the friction, slopes or obstacles that it could overcome when rolling. Further, this study can provide insight into how the design parameters might be tuned in order to improve the mobility of the rover, and help size actuators and sensors for a physical prototype.

*4.1.1 System Description.* The cylindrical version of the TRREx is a multibody system with five bodies; one central frame or "chassis" and the four "legs" that are actuated by motors. The four contacts between the legs and chassis are hinges, thus from Ref. [64], such a system has five degrees of freedom. However, four of these (the motions of the legs) are control inputs, so the only true degree of freedom is the angular position of the chassis. The development of the governing equation for this degree of freedom is presented below and is valid in the no-slip regime.

*4.1.2 Definition of Frames.* A separate reference frame, specified by origin (at the center of mass of that body) and unit axes (aligned in the direction of that body's principle axes) is attached to each body that is moving. In Fig. 5, point $B$ is the center of mass of the chassis (excluding legs) and directions $\hat{i}_{\bar{B}}, \hat{j}_{\bar{B}}$ and $\hat{k}_{\bar{B}}$ ($\hat{k}_{\bar{B}}$ into the plane of the paper) are principle axes directions of the chassis. $\bar{B}$, is a frame with its origin at $B$ and unit axes $\hat{i}_{\bar{B}}, \hat{j}_{\bar{B}}$, and $\hat{k}_{\bar{B}}$. If the legs are numbered 1–4 and have centers of masses $C_1$–$C_4$, respectively, then $\bar{C}_j$ is a frame with its origin at $C_j$ and unit axes $\hat{i}_{\bar{C}_j}, \hat{j}_{\bar{C}_j}$, and $\hat{k}_{\bar{C}_j}$. In addition, an inertial fixed reference frame $\bar{O}$ is defined, whose origin is arbitrary and whose axes are initially aligned with $\bar{B}$.

*4.1.3 Derivation of the Governing Equation.* The total external torque about $B$ acting on the system $\left(\vec{\mathrm{T}}_{B,\mathrm{sys}}\right)_{\mathrm{ext}}$ is related to the change in angular momentum of the system about $B$ [65]

$$\left(\vec{\mathrm{T}}_{B,\mathrm{sys}}\right)_{\mathrm{ext}} = \frac{{}^{\bar{O}}d}{dt}\left({}^{\bar{O}}\vec{h}_{B,\mathrm{sys}}\right) + {}^{\bar{O}}\vec{v}_{B/O} \times m_L \sum_{j=1}^{4} {}^{\bar{O}}\vec{v}_{C_j/O} \tag{8}$$

In above equation, ${}^{\bar{O}}\vec{h}_{B,\mathrm{sys}}$ is the angular momentum of the system about $B$ with respect to the inertial frame, $m_L$ is the mass of each leg, ${}^{\bar{O}}\vec{v}_{B/O}$ is the inertial velocity of the center of mass of the chassis and ${}^{\bar{O}}\vec{v}_{C_jO}$ is the inertial velocity of the center of mass of the $j$th leg. The term ${}^{\bar{O}}\vec{v}_{B/O} \times m_L \sum_{j=1}^{4} {}^{\bar{O}}\vec{v}_{C_j/O}$ appears because the torques and angular momentum are written about a point $B$, which is not the center of mass of the entire system.

The external torques acting on the system can be written as when ground is modeled as flat terrain

$$\left(\vec{\mathrm{T}}_{B,\mathrm{sys}}\right)_{\mathrm{ext}} = \vec{r}_{P/B} \times (\vec{F}_{fr} + \vec{F}_N) + m_L \sum_{j=1}^{4} \left(\vec{r}_{C_j/B} \times \vec{g}\right) \quad (9)$$

$\vec{F}_N$ is the normal reaction, $\vec{F}_{fr}$ is the frictional reaction, and $\vec{F}_R$ is the rolling resistance, as illustrated in Fig. 6.

If the angular velocity of the $\bar{B}$ frame with respect to the $\bar{O}$ frame is written as ${}^{\bar{O}}\vec{\omega}^{\bar{B}} = \omega_{x\bar{B}}\hat{i}_{\bar{B}} + \omega_{y\bar{B}}\hat{j}_{\bar{B}} + \omega_{z\bar{B}}\hat{k}_{\bar{B}}$, since the system is restricted to planar motion about the $\hat{k}_{\bar{B}}$ axis ($\dot{\omega}_{x\bar{B}} = \dot{\omega}_{y\bar{B}} = \omega_{x\bar{B}} = \omega_{y\bar{B}} = 0$), it can be shown [65] that the first term on the right hand side of Eq. (8) reduces to

$$\frac{{}^{\bar{O}}d}{dt}\left({}^{\bar{O}}\vec{h}_{B,\mathrm{sys}}\right) = I_{z\bar{B}}\dot{\omega}_{z\bar{B}}\hat{k}_{\bar{B}} + \sum_{j=1}^{4} I_{z\bar{C}_j}\dot{\omega}_{z\bar{C}_j}\hat{k}_{\bar{C}_j} + m_L \sum_{j=1}^{4}\Big({}^{\bar{B}}\vec{v}_{C_j/B} \times {}^{\bar{O}}\vec{v}_{C_j/O} + {}^{\bar{O}}\vec{\omega}^{\bar{B}} \times \vec{r}_{C_j/B} \times {}^{\bar{O}}\vec{v}_{C_j/O} + \vec{r}_{C_j/B} \times {}^{\bar{O}}\vec{a}_{C_j/O}\Big) \quad (10)$$

where $I_{z\bar{B}}$ and $I_{z\bar{C}_j}$ are the principle inertia components computed about the $\hat{k}_{\bar{B}}$ axis of the chassis and the $\hat{k}_{\bar{C}_j}$ axis of the $j$th leg, respectively, and ${}^{\bar{B}}\vec{v}_{C_j/B}$ and ${}^{\bar{O}}\vec{a}_{C_j/O}$ are the velocity and acceleration of center of mass of the $j$th leg with respect to the $\bar{B}$ and $\bar{O}$ frames, respectively. Now, using Eqs. (9) and (10) in Eq. (8)

$$\vec{r}_{P/B} \times (\vec{F}_{fr} + \vec{F}_N) + m_L \sum_{j=1}^{4}\left(\vec{r}_{C_j/B} \times \vec{g}\right) = I_{z\bar{B}}\dot{\omega}_{z\bar{B}}\hat{k}_{\bar{B}} + \sum_{j=1}^{4} I_{z\bar{C}_j}\dot{\omega}_{z\bar{C}_j}\hat{k}_{\bar{C}_j} + m_L \sum_{j=1}^{4}\Big({}^{\bar{B}}\vec{v}_{C_j/B} \times {}^{\bar{O}}\vec{v}_{C_j/O} + {}^{\bar{O}}\vec{\omega}^{\bar{B}} \times \vec{r}_{C_j/B} \times {}^{\bar{O}}\vec{v}_{C_j/O} + \vec{r}_{C_j/B} \times {}^{\bar{O}}\vec{a}_{C_j/O} + {}^{\bar{O}}\vec{v}_{C_j/O} \times {}^{\bar{O}}\vec{v}_{C_j/O}\Big) \quad (11)$$

Since for the cylindrical system $\hat{k}_{\bar{B}} = \hat{k}_{\bar{C}_j} = \hat{k}_{\bar{O}}$ for all time, the $\hat{k}_{\bar{O}}$ component in Eq. (11) will ultimately yield the equation of motion for the degree of freedom associated with the chassis.

The unknown forces in Eq. (11) can be found using Newton's second law, $\sum \vec{F}_{\mathrm{ext}} = M{}^{\bar{O}}\vec{a}_{B/O} + m_L \sum_{j=1}^{4} {}^{\bar{O}}\vec{a}_{C_j/O}$, where $\sum \vec{F}_{\mathrm{ext}}$ is the sum of external forces acting on the system, $M$ is the mass of the chassis, and ${}^{\bar{O}}\vec{a}_{B/O}$ and ${}^{\bar{O}}\vec{a}_{C_j/O}$ are the inertial accelerations of the center of mass of the chassis and the $j$th leg, respectively. The left hand side gives

$$M\vec{g} + 4m_L\vec{g} + \vec{F}_{fr} + \vec{F}_N + \vec{F}_R = M{}^{\bar{O}}\vec{a}_{B/O} + m_L \sum_{j=1}^{4} {}^{\bar{O}}\vec{a}_{C_j/O} \quad (12)$$

Note that rolling resistance is modeled as a force opposing motion proportional to the magnitude of the normal force

The $\hat{j}_{\bar{O}}$ component in Eq. (12) is used to first solve for the normal force. From this, the rolling resistance can be determined and used in the $\hat{i}_{\bar{O}}$ component to solve for the frictional reaction. This allows for the quantity $(\vec{F}_{fr} + \vec{F}_N)$ to be solved for in Eq. (12) and

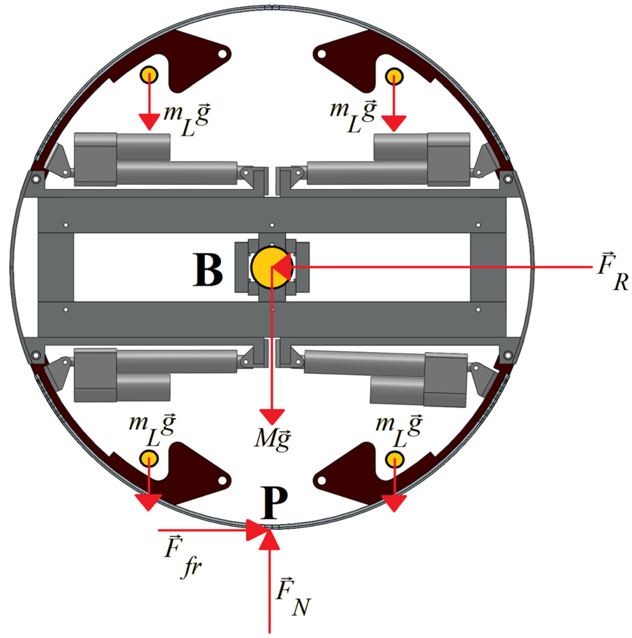


**Fig. 6 External forces on the cylindrical TRREx**

plugged into Eq. (11). The $\hat{k}_{\bar{O}}$ component of Eq. (11) is in terms of system geometric and mass constants and the control inputs of the legs, which are all known. The only unknown is the variable describing rotary motion of the chassis about the $\bar{B}$ frame. Calling this $\theta$, we have $\omega_{z\bar{B}} = \dot{\theta}$ and $\dot{\omega}_{z\bar{B}} = \ddot{\theta}$, thus in Eq. (11) we have a second order differential equation that can be numerically integrated to give chassis motion as a function of time.

*4.1.4 Control Input.* Recalling Fig. 5, if $\gamma_j$ is the angle between the $\hat{i}_{\bar{C}_j}$ and $\hat{i}_{\bar{B}}$ axes in the positive $\hat{k}_{\bar{C}_j}$ direction, then the input motions of the legs are given by $\gamma_j, \dot{\gamma}_j, \ddot{\gamma}_j$. An assumption of this analysis is that the linear motors generate the desired motion exactly, and that the desired angular position of each leg $\gamma_j$ varies from rest position to rest position as a quintic polynomial. If a leg starts at an angular position $\gamma_{\min}$ (fully closed position) and reaches a position $\gamma_{\max}$ (fully open position) in $T$ seconds, then the desired path is chosen such that the initial and final velocities and accelerations are zero. The value of $T$ is set based on the speed of the linear actuator used. The coefficients can be solved from the boundary conditions, and the polynomial describing the desired path of a leg versus time $t$ becomes $\gamma_j(t) = \gamma_{\min} + 10(\gamma_{\max} - \gamma_{\min})(t/T)^3 - 15(\gamma_{\max} - \gamma_{\min})(t/T)^4 + 6(\gamma_{\max} - \gamma_{\min})(t/T)^5$. Given these desired inputs, the governing equation can be numerically integrated using the *ode45* suite in MATLAB® [66].

Continuous rolling motion requires actuating the correct leg at the right time. A controller is developed, to open or close a leg depending on the angular position of the chassis. Thus, ranges where a particular leg should be open are defined. Also to avoid a leg hitting the ground when it is still partially open, these ranges were made to linearly depend on the chassis velocity of rotation. As the velocity of rotation increases, the legs close at an earlier angle so that they have enough time to close completely before the system rolls over that leg.

*4.2 Analysis of Actuated Rolling for the Cylindrical TRREx.* The terrain difficulty for these simulations is characterized by the coefficients of rolling resistance $C_{rr}$ and static friction $\mu_s$. For example, an "easy terrain" would be one that offers low rolling resistance and large enough traction to avoid slip between the rover and the terrain. A "difficult terrain" would be one in which $C_{rr}$ is high and $\mu_s$ is low. As noted before, this model is only valid in the

Table 8 Candidate 1 design parameters

| Parameters | Description | Symbol | Value | Units |
|---|---|---|---|---|
| Geometric parameters | Outer radius of cylindrical surface | $R_w$ | 0.3750 | m |
| | Location of center of mass of leg with respect to hinge | $l_x$ | 0.1961 | m |
| | | $l_y$ | 0.0313 | m |
| | Location of hinge of leg with respect to. center | $h_1$ | 0.3393 | m |
| | | $h_2$ | 0.1275 | m |
| Mass properties | Mass of "chassis" | $M$ | 11.3000 | kg |
| | Mass of each "leg" | $m_L$ | 3.1240 | kg |
| | Inertia about the rotation axis of chassis | $I_{z\bar{B}}$ | 0.8300 | kg m$^2$ |
| | Inertia about the rotation axis of each leg | $I_{z\bar{C}}$ | 0.0394 | kg m$^2$ |

no slip regime (i.e., when $|\vec{F}_{fr}| < \mu_s|\vec{F}_N|$). Thus, after each simulation, it was verified that the system was constantly operating within this regime.

*4.2.1 Earth Simulations.* Anticipating future experimental work on a physical prototype that demonstrates actuated rolling, the authors chose to explore reasonable designs for an Earth prototype. A starting candidate design, as listed in Table 8, was obtained by modeling the system in SolidWorks® and assigning material properties to the components.

First, this design was simulated on "easy terrain" ($C_{rr} = 0.005$, $\mu_s = 0.5$, and $\beta = 0$ deg) and was found to achieve and maintain continuous actuated rolling. For terrains providing little or no opposition to rolling, the actuators on the legs need to be faster because the system rotates faster and the legs have less time to retract. Thus, the maximum speed achieved in actuated rolling is limited by the speed of the actuators that extend/retract the legs.

The next simulation scenario used environmental parameters of $C_{rr} = 0.1$ and $\mu_s = 0.15$ to simulate terrain equivalent to rolling on sand. For these conditions, it was found that the rover would start to roll but would not roll enough for the next leg in sequence to constructively contribute to the perpetuation of rolling motion (called "stall"). To achieve continuous rolling motion on more difficult terrain, the configuration of the rover was changed by (1) pushing each leg's center of mass further from the system center to produce more torque, (2) increasing the inertia of the chassis to reduce the tendency for stall, and (3) increasing the overall mass of the system to reduce the tendency to slip. Updated values for "Candidate 2" were, $l_x = 0.3$ m, $M = 15$ kg, $m_L = 5$ Kg, $I_{z\bar{B}} = 1.5$ kg m$^2$. This updated design was capable of achieving a continuous rolling motion without stalling or slipping on difficult terrain.

To further test the updated design, a gradually inclined "moderate terrain" was generated. Terrain characteristic coefficients of $C_{rr} = 0.05$, $\mu_s = 0.3$, and $\beta = 3$ deg were used to mimic a dirt road or relatively hard sand [67]. Figure 7 shows the results from this simulation. On top, control input is shown as a function of time for the four legs. Below, time-lapse motion is used to show the movement of the center of mass of each leg using a circular marker. The observer in these plots moves along with the system. The top left time-lapse plot shows the system starting from rest, then leg 4 opening and closing before it interferes with the ground. The remaining plots depict how the controller cyclically actuates the legs.

*4.2.2 Mars Simulations.* "Candidate 2" was first subjected to Mars gravity (3.711 m/s$^2$) and terrain parameters of $C_{rr} = 0.1$, $\mu_s = 0.15$, and $\beta = 0$ deg. Results from this simulation showed that the rover had difficulty maintaining a continuous rolling motion because the third leg could not change the angular position of the chassis in such a way that the next leg in the sequence could constructively contribute to the rolling motion. The system stalled in approximately 6 s.

Initial efforts to overcome stall focused on scaling the design so it would have the same weight on Mars that it had on Earth. Trial simulations were slightly better at generating actuated rolling, but were marred by an increased occurrence of slipping. Similar results were found when the leg masses were increased, or when the center of mass of each leg was moved further out from the center of the system. It was found that increasing only the inertia of the rover chassis had three positive effects. First, the system was better able to maintain actuated rolling motion. Second, the tendency to slip was reduced because the inertial accelerations of all the masses were reduced, causing a reduction in the sum of external forces on the system. While the peak of the quantity $\mu_s|\vec{F}_N|$ remained similar, the peak frictional reaction force $|\vec{F}_{\mathrm{fr}}|$ was reduced, meaning that the system was less prone to slip. The third positive effect was that the legs had more time to retract before interfering with the ground because the overall motion of the system was slower.

Thus a design "Candidate 3" was created where all the design parameters were same as "Candidate 2", except the mass of the chassis $M$ was 17.5 Kg and the inertia $I_{z\bar{B}}$ was 2 kg/m$^2$. Simulation results for this system are shown in Fig. 8, where the design is able to maintain continuous actuated rolling motion without stalling or slipping. The top subplot depicts the actuations of the four legs as generated by the controller when it is allowed to run for 15 s. When the value of $\gamma$ for a particular leg is 30 deg (minimum), then that leg is fully closed; when it is 120 deg (maximum), it is in the fully open position. The middle and bottom subplots represent the chassis' angular position and angular velocity, respectively. When actuation is stopped at 15 s and all legs are brought to the fully closed position the system reaches a rest state almost immediately.

**4.3 Discussion.** The candidate designs proposed in the above simulations demonstrate that rover performance using actuated rolling is a function of rover design and the environment in which it operates. These configurations were established through iterative trial and error, and represent only a sampling of the capabilities that the TRREx architecture can achieve. Finding the performance bounds associated with actuated rolling is a source of future work, and will involve a formal design of experiments study to fully sample and characterize the design space.

The linear speeds of the rover in the above simulations under actuated rolling are significant in the context of rover design. The results in Fig. 8 correspond to an average linear speed of 0.19 m/s, which suggests that actuated rolling could be used as a mode of locomotion in conducive environments. In the context of the spherical TRREx design, actuated rolling might be used to roll small distances between slopes to limit the need for transforming between rolling and roving mode. Further, it could also be used to travel over flat or slightly inclined terrain if needed.

## 5 Summary and Conclusions

This paper explored the technical feasibility and performance capabilities of the preliminary TRREx concept. Toward this goal,

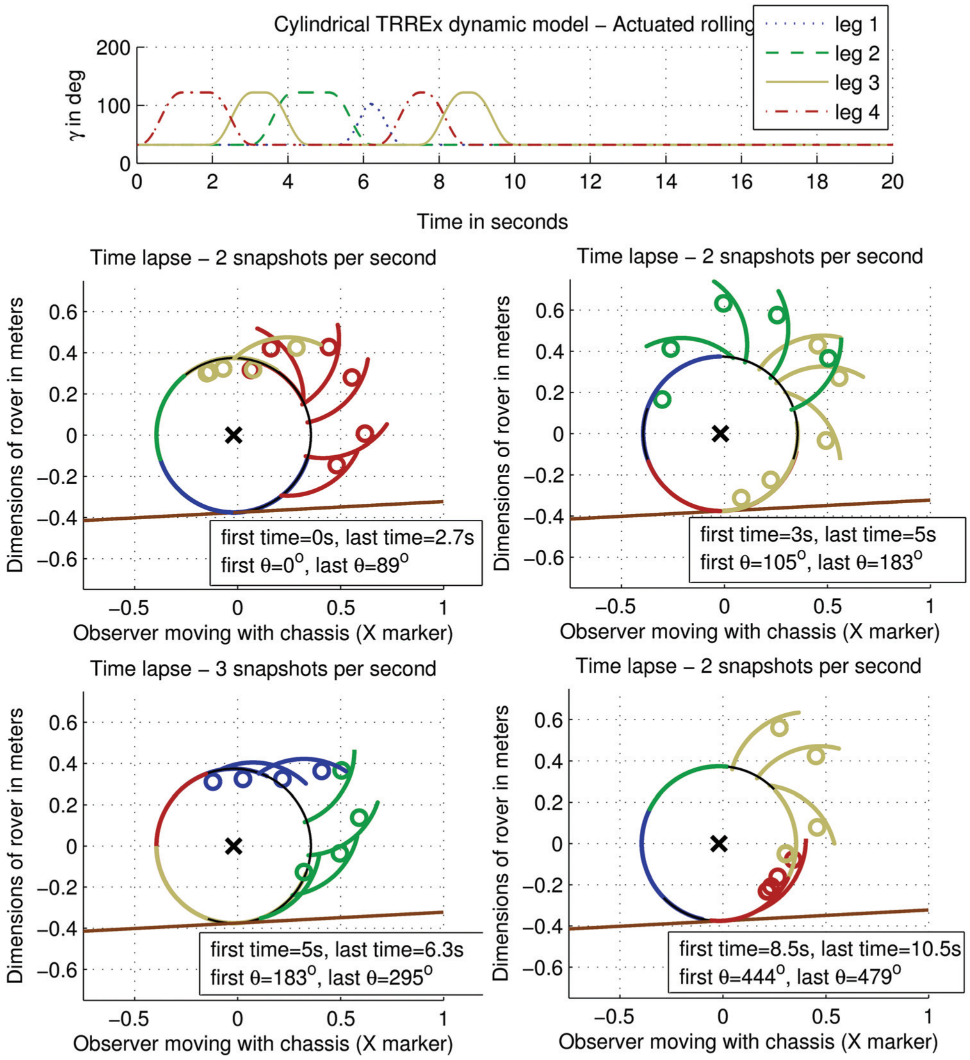


**Fig. 7 Actuated rolling of Candidate 2 up a slope on moderate terrain on Earth**

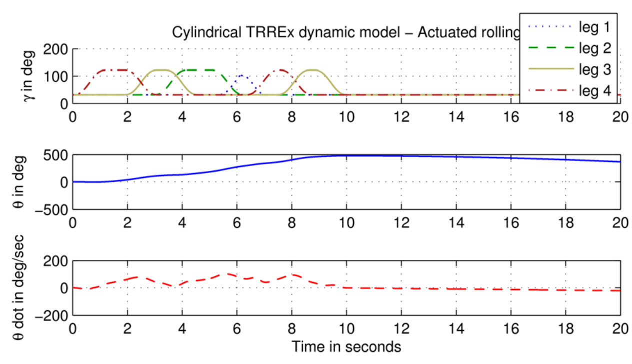


**Fig. 8 Actuated rolling of Candidate 3 on difficult terrain on Mars**

Sec. 3 used a hi-fidelity simulation engine provided by the Webots software package to assess initial performance. This simulation engine used random rock fields and returned raw data that was analyzed and assessed for three performance measures. As the rover concepts are further developed, more sophisticated Solidworks models should be constructed. Additionally, simulation fidelity can be improved by using more realistic rock fields with varied geometries and heights, and a ground interaction model that includes a sinking mode.

In the simulations conducted the TRREx rover typically underperformed the rocker-bogie on flat terrain, but demonstrated potential improvements on both uphill and downhill courses. For many of the individual trials, the choice of weighting parameters for performance aggregation did not change the winning outcome. The size parameter indicated that large rovers are good for relatively benign terrain. However, small rovers may be better for very rugged scenarios as their shorter turning diameters may allow them to navigate around rocks that are too big to cross, even for very large rovers. However, size decisions may be constrained depending on criteria associated with payload weight and size.

At the mission level, it was found that the choice of weights did cause a rank reversal. Further, missions with downhill components and dense rock fields demonstrated performance advantages of the TRREx that warranted further development of the concept. However, strong statements about architecture dominance cannot be made given the construction of the study. Future work should explore additional performance measures (cost, risk, etc.), study the robustness of the best alternative by exploring how changes to the Strength of Preference curves influence the final outcome, and use a nonweighted scheme to explore the solution space.

Section 4 further developed the TRREx concept by exploring system dynamics and performance capabilities associated with actuated rolling. A cylindrical model of the TRREx was generated that had four actuated legs. A controller was designed that generated actuation inputs based on the system's angular position and velocity. Ground interference was avoided by making the opening and closing ranges of the legs a function of velocity and position.

Simulations demonstrated that maintaining a continuous actuated rolling motion depended on the rover design and the operating environment. In the Earth environment it was shown that actuated rolling could be used to traverse a gradual incline. Future work from these simulations should focus on developing a physical prototype of the cylindrical model for testing and validation. Results in a Mars environment showed that actuated rolling gives the TRREx the capacity to self-propel and that it could be used as the primary mode of locomotion if necessary. To further develop this concept, future work should sample the design space to understand performance bounds for different terrains and extend the cylindrical model to a 3D representation of the system.

## Acknowledgment

We gratefully acknowledge support from the NASA Innovative Advanced Concepts Program through NASA Grant No. NNX11AR26G.

## References

[1] Muirhead, B. K., 2004, "Mars Rovers, Past and Future," Proceedings of the IEEE Aerospace Conference, pp. 6–13.
[2] Kilit, O., and Yontar, A., 2009, "Stability of a New Mars Rover With Multi-Stage Bogie Mechanism," 4th International Conference on Recent Advances in Space Technologies, Istanbul, Turkey, pp. 145–149.
[3] Kite, E. S., Rafkin, S. Michaels, T., Dietrich, W. E., and Manga, M., 2011, "Chaos Terrain, Storms, and Past Climate on Mars," J. Geophys. Res.-Planets, **116**, p. E100002.
[4] Eisen, H. J., Buck, C. W., Gillis-Smith, G. R., and Umland, J. W., 1997, "Mechanical Design of the Mars Pathfinder Mission," Proceedings of Seventh European Space Mechanisms and Tribology Symposium, ESA Headquarters, Noordwijk, Netherlands, pp. 11–17.
[5] Lindemann, R. A., Bickler, D. B., Harrington, B. D., Ortiz, G. M., and Voorhees, C. J., 2006, "Mars Exploration Rover Mobility Development–Mechanical Mobility Hardware Design, Development, and Testing," IEEE Rob. Autom. Mag., **13**(2), pp. 19–26.
[6] Golombek, M., Arvidson, R. E., Bell, J. F., Christensen, P. R., Crisp, J. A., Crumpler, L. S., Ehlmann, B. L., Fergason, R. L., Grant, J. A., Greeley, R., Haldemann, A. F. C., Kass, D. M., Parker, T. J., Schofield, J. T., Squyres, S. W., and Zurek, R. W., 2005, "Assessment of Mars Exploration Rover Landing Site Predictions," Nature, **436**(7047), pp. 44–48.
[7] Siegwart, R., Lamon, P., Estier, T., Lauria, M., and Piguet, R., 2002, "Innovative Design for Wheeled Locomotion in Rough Terrain," Rob. Auton. Syst., **40**(2–3), pp. 151–162.
[8] Miller, D. P., and Tze-Liang, L., 2002, "High-Speed Traversal of Rough Terrain Using a Rocker-Bogie Mobility System," Space 2002 and Robotics 2002: Proceedings of Space 2002: The Eighth International Conference and Exposition on Engineering, Construction, Operations, and Business in Space, and Proceedings of Robotics 2002: The Fifth International Conference and Exposition/Demonstration on Robotics for Challenging Situations and Environments, Albuquerque, NM.
[9] Lindemann, R. A., and Voorhees, C. J., 2005, "Mars Exploration Rover Mobility Assembly Design, Test, and Performance," 2005 IEEE Conference on Systems, Man and Cybernetics, The Big Island, HI, Vol. 1, pp. 450–455.
[10] Edwin, L. E., Mazzoleni, A. P., and Hartl, A. E., 2012, "Biologically Inspired Transforming Roving-Rolling Explorer (TRREx) Rover for Lunar Exploration," Proceedings of the 63rd International Astronautical Congress, Naples, Italy, Paper IAC-12.A3.2D.12.
[11] Ferguson, S., Lewis, K., de Weck, O., and Siddiqi, A., 2007, "Flexible and Reconfigurable Systems: Nomenclature and Review," 2007 ASME DETC and CIE Conferences, Las Vegas, NV, Sept. 4–7, ASME Paper No. DETC2007/DAC-35745, pp. 249–263.
[12] Singh, V., Skiles, S., Krager, J., Wood, K., Jensen, D., and Sierakowski, D., 2009, "Innovations in Design Through Transformation: A Fundamental Study of Transformation Principles," ASME J. Mech. Des., **131**(8), pp. 1–18.
[13] Haldaman, J., 2010, "Study of Reconfigurability and Reconfigurable Products for Use in Design," M.S. thesis, Penn State University, University Park, PA.
[14] Haldaman, J., and Parkinson, M., 2010, "Reconfigurable Products and Their Means of Reconfiguration," 2010 ASME International Design Engineering Technical Conferences and Computers and Information in Engineering Conference, Quebec, Canada, Aug. 15–18, ASME Paper No. DETC2010-28528, pp. 219–228.
[15] Olewnik, A., Brauen, T., Ferguson, S., and Lewis, K., 2004, "A Framework for Flexible Systems and Its Implementation in Multiattribute Decision Making," ASME J. Mech. Des., **126**(3), pp. 412–419.
[16] Siddiqi, A., de Weck, O., and Iagnemma, K., 2006, "Reconfigurability in Planetary Surface Vehicles: Modeling Approaches and Case Study," J. Br. Interplanet. Soc., **59**(12): 450–460.
[17] Neches, R., 2011, "Engineered Resilient Systems S&T Priority Description and Roadmap," Proceedings of the NDIA 8th Annual Disruptive Technologies Conference, Washington D.C.
[18] Madni, A., and Jackson, S., 2009, "Towards a Conceptual Framework for Resilience Engineering," IEEE Syst. J., **3**(2), pp. 181–191.
[19] Namgoong, H., Crossley, W. A., and Lyrintzis, A. S., 2012, "Morphing Airfoil Design for Minimum Drag and Actuation Energy Including Aerodynamic Work," J. Aircr., **49**(4), pp. 981–990.
[20] Bowman, J., Weisshaar, T., and Sanders, B., 2002, "Evaluating the Impact of Morphing Technologies on Aircraft Performance," 43rd AIAA/ASME/ASCE/AHA/ACS Structures, Structural Dynamics, and Materials Conference, Denver, CO, AIAA 2002–1631.
[21] Ferguson, S., Kasprzak, E., and Lewis, K., 2008, "Designing a Family of Reconfigurable Vehicles Using Multilevel Multidisciplinary Design Optimization," Struct. Multidiscip. Optim., **39**(2), pp. 171–186.
[22] Olewnik, A., and Lewis, K., 2006, "A Decision Support Framework for Flexible System Design," J. Eng. Des., **17**(1), pp. 75–97.
[23] Khire, R., and Messac, A., 2008, "Selection-Integrated Optimization (SIO) Methodology for Optimal Design of Adaptive Systems," ASME J. Mech. Des., **130**(10), p. 101401.
[24] Chmarra, M., Waarsing, R., Verriet, J., and Tomiyama, T., 2010, "State Transition in Reconfigurable Systems," 2010 ASME International Design Engineering Technical Conferences and Computers and Information in Engineering Conference, Quebec, Canada, Aug. 15–18, ASME Paper No. DETC2010–28723.
[25] Siddiqi, A., and de Weck, O., 2008, "Modeling Methods and Conceptual Design Principles for Reconfigurable Systems," ASME J. Mech. Des., **130**(10), p. 101102.
[26] Arts, L., Chmarra, M., and Tomiyama, T., 2008, "Modularization Method for Adaptable Products," 2008 ASME International Design Engineering Technical Conference and Computers and Information in Engineering Conference, New York, NY, Aug. 3–6, ASME Paper No. DETC2008-49338.
[27] Lewis, P., and Mattson, C., 2011, "A Method for Developing Systems that Traverse the Pareto Frontiers of Multiple System Concepts Through Modularity," Struct. Multidiscip. Optim., **45**(4), pp. 467–478.
[28] Lewis, P., Murray, V., and Mattson, C., 2011, "A Design Optimization Strategy for Creating Devices That Traverse the Pareto Frontier Over Time," Struct. Multidiscip. Optim., **43**(2), pp. 191–204.
[29] Chmarra, M., Arts, L., and Tomiyama, T., 2008, "Towards Adaptable Architecture," 2008 ASME International Design Engineering Technical Conference and Computers and Information in Engineering Conference, New York, NY, Aug. 3–6, ASME Paper No. DETC2008-49971.
[30] Pate, D., Patterson, M., and German, B., 2012, "Optimizing Families of Reconfigurable Aircraft for Multiple Missions," J. Aircr., **49**(6): 1988–2000.
[31] Patterson, M., Pate, D., and German, B., 2012, Performance Flexibility of Reconfigurable Families of Unmanned Air Vehicles," J. Aircr., **49**(6), pp. 1831–1843.
[32] Simpson, T., Siddique, Z., and Jiao, J., eds., 2006, *Product Platform and Product Family Design: Methods and Applications*, Springer, New York.
[33] Jiao, J., Simpson, T., and Siddique, Z., 2007, "Product Family Design and Platform-Based Product Development: A State-of-the-Art Review," J. Intell. Manuf., **18**(1), pp. 5–29.
[34] Pirmoradi, Z., and Wang, G., 2011, "Recent Advancements in Product Family Design and Platform-Based Product Development: A Literature Review," 2011 ASME International Design Engineering Technical Conference and Computers and Information in Engineering Conference, Washington, DC, Aug. 28–31, ASME Paper No. DETC2011–47959, pp. 1041–1055.
[35] Ferguson, S., and Lewis, K., 2006, "Effective Development of Reconfigurable Systems Using Linear State-Feedback Control," AIAA J., **44**(4), pp. 868–878.
[36] McGowan, A., Vicroy, D., Busan, R., and Hahn, S., 2009, "Perspectives on Highly Adaptable or Morphing Aircraft," RTO Applied Vehicle Technology Panel (AVT) Symposium, Evora, Portugal.
[37] Yen, J., Jain, A., and Balaram, J., 1999, "ROAMS: Rover Analysis Modeling and Simulation," 5th International Symposium on Artificial Intelligence, Robotics and Automation in Space, Noordwijk, Netherlands.
[38] Michaud, S., Richter, L., Thueer, T., Gibbesch, A., Huelsing, T., Schmitz, N., Weiss, S., Krebs, A., Patel, N., Joudrier, L., Siegwart, R., Schafer, B., and Ellery, A., 2006, "Rover Chassis Evaluation and Design Optimization Using the RCET," Proceedings of the 9th ESA Workshop on ASTRA, Noordwijk, Netherlands.
[39] Michaud, S., Richter, L., Patel, N., Thueer, T., Huelsing, T., Joudrier, L., Siegwart, R., and Ellery, A., 2004, "RCET: Rover Chassis Evaluation Tools," Proceedings of the 8th ESA Workshop on ASTRA, Noordwijk, Netherlands.
[40] Sohl, G., and Jain, A., 2005, "Wheel-Terrain Contact Modeling in the ROAMS Planetary Rover Simulation," Proceedings of the ASME International Design Engineering Technical Conferences and Computers and Information in Engineering Conference, Vol. 6(A–C), pp. 89–97.
[41] Yang, Y. C., Bao, J. S., Jin, Y., and Cheng, Y. L., 2008, "A Virtual Simulation Environment for Lunar Rover: Framework and Key Technologies," Int. J. Adv. Rob. Syst., 5(2), pp. 201–208.
[42] Patel, N., Ellery, A., Allouis, E., Sweeting, M., and Richter, L., 2004, "Rover Mobility Performance Evaluation Tool (RMPET): A Systematic Tool for Rover Chassis Evaluation Via Application of Bekker Theory," Proceedings of the 8th ESA Workshop on Advanced Space Technologies for Robotics and Automation, Noordwijk, Netherlands.
[43] Webots, Commercial Mobile Robot Simulation Software, http://www.cyberbotics.com

[44] Michel, O., 2004, "WebotsTM: Professional Mobile Robot Simulation," Int. J. Adv. Robotic Syst., **1**(1), pp. 39–42.
[45] Wang, L. F., Tan, K. C., and Prahlad, V., 2002, "Developing Khepera Robot Applications in a Webots Environment," International Symposium on Micromechatronics and Human Science, Nagoya, Japan.
[46] Open Dynamics Engine, www.ode.org
[47] Genta, G., and Genta, A., 2011, "Preliminary Assessment of a Small Robotic Rover for Titan Exploration," Acta Astronaut., 68(5–6), pp. 556–566.
[48] Bauer, R., Barfoot, T., Leung, W., and Ravindran, G., 2008, "Dynamic Simulation Tool Development for Planetary Rovers," Int. J. Adv. Rob. Syst., 5(3), pp. 311–314.
[49] Bruhn, F. C., Kratz, H., Warell, J., et al., 2008, "A Preliminary Design for a Spherical Inflatable Microrover for Planetary Exploration," Acta Astronaut., 63(5–6), pp. 618–631.
[50] Chen, F., and Genta, G., 2012, "Dynamic Modeling of Wheeled Planetary Rovers: A Model Based on the Pseudo-Coordinates Approach," Acta Astronaut., 81, pp. 288–305.
[51] Chen, B. C., Wang, R. B., Jia, Y., Guo, L., and Yang, L., 2009, "Design of a High Performance Suspension for Lunar Rover Based on Evolution," Acta Astronaut., 64(9–10), pp. 925–934.
[52] Hacot, H., Dubowsky, S., and Bidaud, P., 1998, "Analysis and Simulation of a Rocker-Bogie Exploration Rover," Courses and Lectures—International Centre for Mechanical Sciences, pp. 95–102.
[53] Perko, H., Nelson, J., and Green, J., 2006, "Mars Soil Mechanical Properties and Suitability of Mars Soil Simulants," J. Aerosp. Eng., **19**(3), pp. 169–176.
[54] Golombek, M., and Rapp, D., 1997, "Size-frequency Distributions of Rocks on Mars and Earth Analog Sites: Implications for Future Landed Missions," J. Geophys. Res.—Planets, **102**(E2), pp. 4117–4129.
[55] Genta, G., 2011, *Introduction to the Mechanics of Space Robots*, Springer Science Business Media, New York.
[56] Otto, K. N., and Antonsson, E. K., 1991, "Trade-Off Strategies in Engineering Design," Res. Eng. Des., **3**(2), pp. 87–103.
[57] Lewis, K. E., Chen, W., and Schmidt, L. C., 2006, *Decision Making in Engineering Design*, ASME Press, New York.
[58] Hazelrigg, G., 1998, "A Framework for Decision-Based Engineering Design," ASME J. Mech. Des., **120**(4), pp. 653–658.
[59] See, T.-K., Gurnani, A., and Lewis, K., 2005, "Multi-Attribute Decision Making Using Hypothetical Equivalents and Inequivalents," ASME J. Mech. Des., **126**(6), pp. 950–958.
[60] Wilson, J. L., Mazzoleni, A. P., and DeJarnette, F. R., 2008, "Design, Analysis and Testing of Mars Tumbleweed Rover Concepts," J. Spacecr. Rockets, **45**(2), pp. 370–382.
[61] Hartl, A. E., and Mazzoleni, A. P., 2010, "Dynamic Modeling of a Wind-Driven Tumbleweed Rover Including Atmospheric Effects," J. Spacecr. Rockets, **47**(3), pp. 493–502.
[62] Hartl, A. E., and Mazzoleni, A. P., 2012, "Terrain Modeling and Simulation of a Tumbleweed Rover Traversing Martian Rock Fields," J. Spacecr. Rockets, **49**(2), pp. 401–412.
[63] Hartl, A. E., and Mazzoleni, A. P., 2008, "Parametric Study of Spherical Rovers Crossing a Valley," J. Guid., Control, Dyn., **31**(3), pp. 775–778.
[64] Uicker, J. J., Pennock, G., and Shigley, J., 2003, *Theory of Machines and Mechanisms*, Oxford University, MA.
[65] Meirovitch, L., 2003, *Methods of Analytical Dynamics*, Dover, Mineola, NY.
[66] MATLAB version 7.10.0.499, 2010, *Natick*, The MathWorks Inc., MA.
[67] Baker, I. O., 1919, *A Treatise on Roads and Pavements*, John Wiley & Sons, New York.